High Q-Factor Diamond Optomechanical Resonators with Silicon Vacancy Centers at Millikelvin Temperatures

Joe, Graham; Chia, Cleaven; Pingault, Benjamin; Haas, Michael; Chalupnik, Michelle; Cornell, Eliza; Kuruma, Kazuhiro; Machielse, Bartholomeus; Sinclair, Neil; Meesala, Srujan

DOI
10.1021/acs.nanolett.3c04953

Publication date
2024

Document Version
Final published version

Published in
Nano Letters

Citation (APA)
Joe, G., Chia, C., Pingault, B., Haas, M., Chalupnik, M., Cornell, E., Kuruma, K., Machielse, B., Sinclair, N., Meesala, S., & Lončar, M. (2024). High Q-Factor Diamond Optomechanical Resonators with Silicon Vacancy Centers at Millikelvin Temperatures. *Nano Letters*, *24*(23), 6831-6837. https://doi.org/10.1021/acs.nanolett.3c04953

NANO LETTERS

pubs.acs.org/NanoLett

Letter

High *Q*-Factor Diamond Optomechanical Resonators with Silicon Vacancy Centers at Millikelvin Temperatures

Graham Joe,[▽] Cleaven Chia,[▽] Benjamin Pingault, Michael Haas, Michelle Chalupnik, Eliza Cornell, Kazuhiro Kuruma, Bartholomeus Machielse, Neil Sinclair, Srujan Meesala, and Marko Lončar*

Cite This: *Nano Lett.* 2024, 24, 6831−6837

Read Online

ACCESS | Metrics & More | Article Recommendations | Supporting Information

ABSTRACT: Phonons are envisioned as coherent intermediaries between different types of quantum systems. Engineered nanoscale devices, such as optomechanical crystals (OMCs), provide a platform to utilize phonons as quantum information carriers. Here we demonstrate OMCs in diamond designed for strong for interactions between phonons and a silicon vacancy (SiV) spin. Using optical measurements at millikelvin temperatures, we measure a line width of 13 kHz (*Q*-factor of ∼4.4 × 10^5) for a 6 GHz acoustic mode, a record for diamond in the GHz frequency range and within an order of magnitude of state-of-the-art line widths for OMCs in silicon. We investigate SiV optical and spin properties in these devices and outline a path toward a coherent spin−phonon interface.

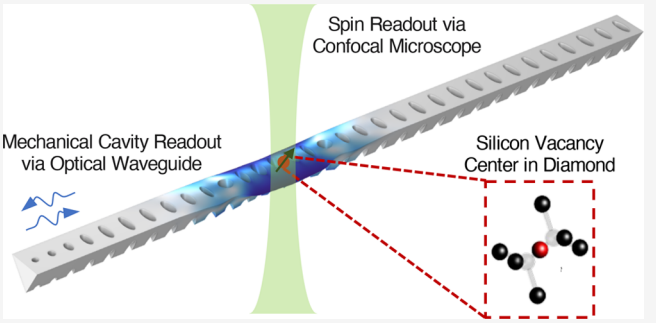

KEYWORDS: *optomechanics, silicon vacancy, diamond, phonons*

Micro/nanomechanical systems have emerged as a promising platform for quantum science and technology owing to their ability to coherently interact with a wide variety of quantum systems.[1−3] Optomechanical crystals (OMCs), which confine optical photons and acoustic phonons on a wavelength scale and thus can enable efficient photon−phonon interactions,[4] have attracted significant attention. The optomechanical interaction has been used to demonstrate quantum ground-state cooling of a macroscopic mechanical mode,[5] squeezed light,[6] microwave-to-optical transduction,[7] and a telecom spin−photon interface using an intermediary mechanical mode,[8] as depicted in Figure 1(a). Wavelength-scale confinement of phonons in OMCs could also allow for strong coupling between a mechanical mode and a strain-sensitive defect spin qubit.[9] Single-crystal diamond is a natural platform for such devices since it hosts a variety of color-center spin qubits and features low mechanical dissipation, large Young's modulus, and a wide optical transparency window.[10−12] This has motivated activity on coherent acoustic driving of nitrogen vacancy (NV) spins in a variety of diamond-based devices such as bulk-acoustic resonators and cantilevers.[2,13−15] Relative to the NV center, the silicon vacancy center (SiV) in diamond is better suited as a spin−phonon interface since it provides nearly 4 orders of magnitude higher strain susceptibility (∼100 THz/strain) for the ground state spin.[9,16] Recently, this has been leveraged to demonstrate low power and coherent acoustic control of a single SiV spin and proximal nuclear spins.[3,17] Importantly, the SiV maintains good optical properties in nanofabricated structures in terms of its narrow zero-phonon line (ZPL) and spectral stability, which allow for high fidelity and high efficiency spin−photon entanglement generation.[18] OMCs in diamond have been demonstrated and proposed to enhance the spin−phonon interaction strength toward the strong spin−phonon coupling regime.[19,20] However, their performance at millikelvin temperatures and their compatibility with SiV centers have not yet been investigated. Operation in this temperature regime is crucial to maintain good SiV spin coherence, improve mechanical quality factors, and thereby achieve high cooperativity spin−phonon interactions capable of operating near the single-phonon regime.

In this work, we report diamond OMCs which support optical and mechanical modes measured at f_{opt} = 189.6 THz (1580.8 nm) and f_{mech} = 5.76 GHz with high quality factors of Q_{opt} ∼ 15,000 and Q_{mech} ∼ 440,000, respectively, measured at millikelvin temperatures. These OMCs have a large simulated zero-point mechanical fluctuation of x_{zpf} = 3.58 fm, an effective motional mass of 158 fg, and an expected spin−phonon coupling strength (g_{sp}) of up to 1.65 MHz, which is large

Received: December 15, 2023
Revised: March 11, 2024
Accepted: March 12, 2024
Published: May 30, 2024

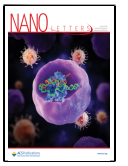

https://doi.org/10.1021/acs.nanolett.3c04953
Nano Lett. 2024, 24, 6831−6837

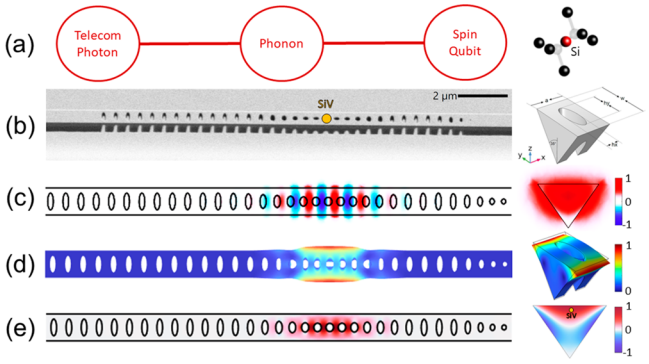

Figure 1. (a) Illustration of the coupled optical, mechanical, and spin degrees of freedom in the SiV-OMC devices. The inset shows the atomic structure of the SiV center in diamond. (b) Scanning electron micrograph of a typical diamond OMC device fabricated by an angled etching technique. The location of the SiV center is indicated with an orange dot. The inset shows the schematic of a unit cell of diamond optomechanical crystals with geometric parameters of (a, w, h_x, h_y) = (528, 936, 197, 578) nm and a bottom apex half angle of $\theta = 35°$. (c) Optical mode profile (E_y component) of the fundamental quasi-transverse electric (TE) mode at f_{opt} = 197.2 THz (λ_{opt} = 1520 nm). The inset shows the cross-sectional profile of the optical mode. (d) Displacement and (e) strain profile of the mechanical (flapping) mode supported by the OMC device at f_{mech} = 6.6 GHz. The insets of parts d and e show the 3D displacement profile of a unit cell and the cross-sectional strain profile, respectively.

relative to our measured mechanical line width (13 ± 1 kHz) and previously measured SiV spin decoherence rates (~100 Hz).[21] The diamond OMCs were fabricated with an angled etching technique.[22] By measuring the dependence of the mechanical line width on the optical pump power, we inferred an optomechanical coupling strength of $g_{OM}/2\pi \sim 30.3 \pm 1.6$ kHz at the single photon and phonon level. We characterized single SiV centers embedded in these high-Q diamond OMCs and observed excellent optical properties. However, we observed a reduced spin lifetime (T_1) of SiV centers in OMCs compared with expected values,[21] likely due to optically induced local heating. Such heating, caused by parasitic optical absorption, has previously been noted as a source of excess acoustic damping in OMCs at millikelvin temperatures.[23,24] We discuss alternative OMC device architectures to mitigate the impact of optically induced heating on spin and mechanical properties.

Our diamond OMCs consist of a free-standing diamond waveguide with triangular cross-section[22] and a one-dimensional (1D) array of elliptical air-holes [Figure 1(b)]. To form photonic and phononic cavities in the same region, we locally vary the lattice constant and eccentricity of the air-holes. Details of the tapering method can be found in the Supporting Information. The optical and mechanical modes of diamond OMCs are then simulated using the finite-difference time-domain (FDTD) method (Lumerical) and the finite element method (FEM) (COMSOL). Figure 1(c) shows the field distribution of a quasi-transverse electric (TE) optical resonance at λ_{opt} = 1520 nm. The calculated Q_{opt} and mode volume are 5×10^6 and $0.50(\lambda_{opt}/n)^3$, respectively, where n = 2.4 is the refractive index of diamond. The designed OMC also supports a so-called "flapping" mode [Figure 1(d)], with a large zero-point motion x_{zpf} of 3.58 fm at 6.6 GHz. This mode has large mechanical displacements near the edge of the cavity region and large strain fields near the center [Figure 1(e)], making it possible to achieve large optomechanical coupling to a quasi-TE optical mode.[19] The maximum strain amplitude and optimal SiV spin location are in the center of the waveguide between the holes of the cavity region and close to

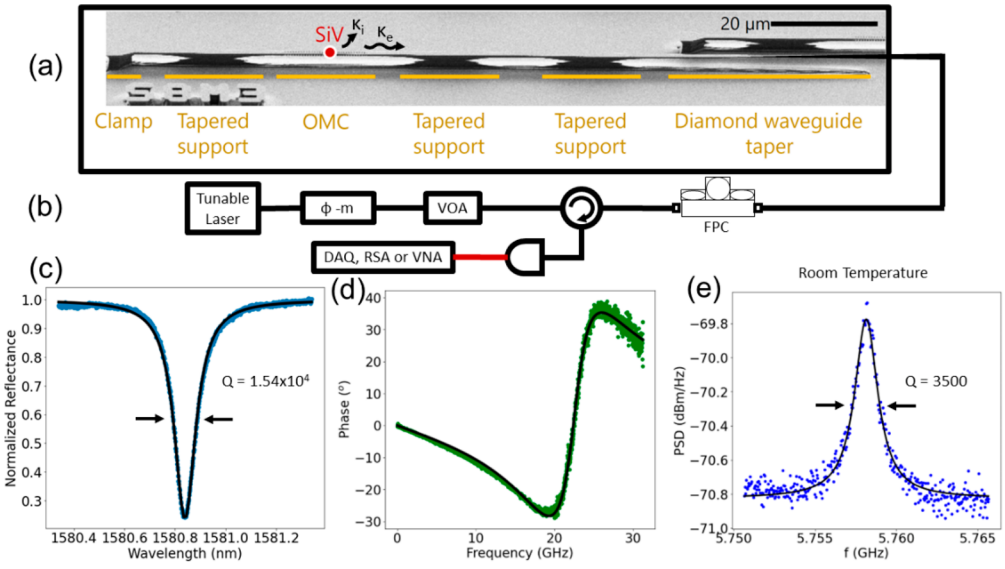

Figure 2. Room temperature characterization of diamond OMC. (a) SEM of a diamond OMC device with a tapered waveguide for adiabatic coupling with a tapered optical fiber. Our optical cavities are designed to be a single-side waveguide coupled with an extrinsic coupling rate κ_e and an intrinsic optical loss rate κ_i. (b) Simplified schematic of the characterization setup. Φ-m, electro-optic phase modulator; VOA, variable optical attenuator; DAQ, data acquisition device; RSA, real-time spectrum analyzer; VNA, vector network analyzer. (c) Normalized reflection spectrum of the OMC optical mode. A Lorentzian fit (black curve) yields λ_{opt} = 1580.8 nm and a line width of 12.3 GHz (total optical Q-factor of 1.54×10^4). (d) Phase response of the optical resonance. $\kappa_e/(2\pi) \sim 9$ GHz is obtained by fitting (black curve). (e) Power spectral density (PSD) of the mechanical "flapping" mode measured on the RSA with laser detuning of $\Delta = -\kappa/2$. A Lorentzian fit yields a mechanical line width of 1.63 MHz (mechanical Q-factor of 3500).

https://doi.org/10.1021/acs.nanolett.3c04953
Nano Lett. 2024, 24, 6831−6837

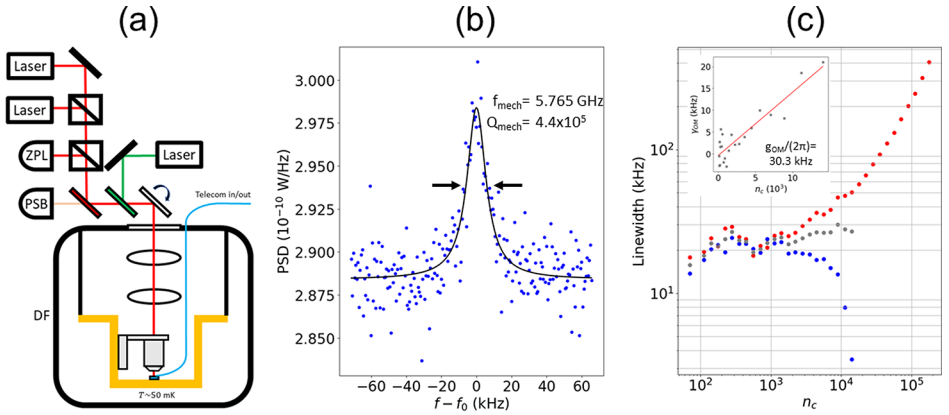

Figure 3. Millikelvin temperature characterization of diamond OMCs. (a) Schematic of the dilution refrigerator setup and optical path. SiV centers are measured with a confocal microscope built on top of the cryostat. A single-ended tapered optical fiber is used to couple telecom wavelength light into the OMC device of interest. Two lasers are used to address the SiV spin-selective optical transitions, and a pulsed green laser is used as a charge repump for the SiV. Zero-phonon line (ZPL) and phonon sideband (PSB) emission are collected on separate avalanche photodiodes. (b) Mechanical mode spectrum of an OMC device measured at ∼50 mK with the probe laser parked on the blue sideband ($\Delta = \kappa/2$) at low input power ($n_c \sim 100$). The mechanical line width is 13 ± 1 kHz, corresponding to a mechanical Q-factor of 4.4×10^5. (c) Mechanical line width of the OMC device as a function of intracavity photon number n_c. Blue (red) points are the experimental data taken with the laser tuned to the blue (red) optomechanical sideband of the cavity ($\Delta = \pm\kappa/2$). Gray circles indicate the intrinsic mechanical line width (γ_i) values and are obtained by taking the average of the red and blue detuned data points. The inset shows the calculated optomechanically induced damping ($\gamma_{OM} = \gamma_{red} - \gamma_i$); a linear fit yields $g_{OM}/2\pi \sim 30.3 \pm 1.6$ kHz.

the top surface of the device. The details of the cavity simulation can be found in the Supporting Information.

Given the calculated profiles of optical and mechanical modes, we estimate the optomechanical coupling rate between the optical mode and the mechanical flapping mode $g_{OM}/2\pi$ to be 127 kHz. This value is comparable with the values previously reported in diamond OMCs at similar frequencies.[19] We also calculated the spin−phonon coupling rate g_{sp} from the simulated mechanical flapping mode assuming a single SiV is coupled to the maximum strain located at a depth of 20 nm below the diamond surface [see inset in Figure 1(d)]. The maximum achievable $g_{sp}/2\pi$ at this implantation depth is 1.65 MHz.

The OMCs are fabricated on electronic-grade single-crystal diamond substrates (Element Six). The OMC fabrication process, previously described in ref 25, consists of the following steps: (i) patterning of alignment markers, (ii) generation of SiV centers at a 20 nm depth via masked implantation and annealing,[26,27] (iii) OMC fabrication via vertical and angled etching.[22] Steps (ii) and (iii) are performed aligned to the markers defined in (i) (see the Supporting Information for more details of the fabrication process). For this sample, silicon ions are implanted in the diamond substrate with a dose of $1.25 \times 10^{12}/\text{cm}^2$ and a beam energy of 27.5 keV. The sample is then annealed at ∼1400 K in an ultrahigh vacuum furnace at pressures $<10^{-6}$ Torr to activate SiV centers. Figure 2(a) shows a scanning electron microscopy (SEM) image of the fabricated OMCs. The structure incorporates a tapered waveguide region at its end (right side) for high optical coupling efficiency to a tapered optical fiber.[28] To mechanically support the OMC and thermally anchor it to the cold bath of the diamond substrate for cryogenic experiments, we introduced two adiabatically widened anchors, designed to have low scattering loss, between the OMC and the tapered waveguide and one on the other side between the OMC and the clamp [Figure 3(a)].

We performed room temperature characterization of the fabricated OMCs using a home-built optical fiber coupling setup,[19] illustrated in Figure 2(b). We investigate the optical mode of the optical mode of the OMC by measuring the reflection spectrum [Figure 2(c)] with an ∼1550 nm tunable laser source coupled via the tapered waveguide−tapered optical fiber interface. We fit the resonance with a Lorentzian function and obtained a line width of $\kappa/2\pi$ = 12.34 GHz (corresponding to an optical Q of 15,400). To determine whether the cavity Q is limited by intrinsic or extrinsic losses, we measured the phase response of the cavity mode.[29] This is accomplished by detuning the probe laser from the cavity resonance by 0.18 nm (21.3 GHz) and then sweeping a sideband generated by an electro-optic (EO) phase modulator across the cavity resonance. The resulting RF beat note of the reflected optical power is recorded on a high bandwidth photodiode connected to a vector network analyzer (VNA). Figure 2(d) shows the phase response of the optical resonance. Using κ extracted from the cavity reflection spectrum, a fit to the phase response allows us to extract intrinsic and extrinsic cavity loss rates $(\kappa_i, \kappa_e)/2\pi$ = (3.17, 9.17) GHz, where $\kappa = \kappa_i + \kappa_e$. We can therefore conclude that our optical cavity is overcoupled, deviating somewhat from the targeted critical coupling condition (Supporting Information). For mechanical mode spectroscopy, we set the probe laser detuning from the cavity resonance (Δ) to $\pm\kappa/2$ where displacement sensitivity is maximum; we then measured the RF modulation of the probe laser due to the thermal occupation of the mechanical mode.[30] The reflected signal is detected by a high bandwidth photodetector connected to a real-time spectrum analyzer [Figure 2(b)]. Figure 2(e) shows the power spectral density (PSD) of the "flapping" mechanical mode measured at room temperature. By fitting the PSD to a Lorentzian function, a room temperature mechanical quality factor of $Q_{mech} \sim 3500$ is measured (in air), likely limited by multiphonon damping mechanisms.[31] Given the measured optical cavity loss rate (κ = 12.34 GHz) and the frequency of the targeted mechanical mode ($f_{mech} \sim 5.76$ GHz), our OMC system is in the sideband unresolved regime, where a probe laser detuning of $\Delta = \pm\kappa/2$ is optimal.[32] Future improvements in fabrication may enable us

https://doi.org/10.1021/acs.nanolett.3c04953
Nano Lett. 2024, 24, 6831−6837

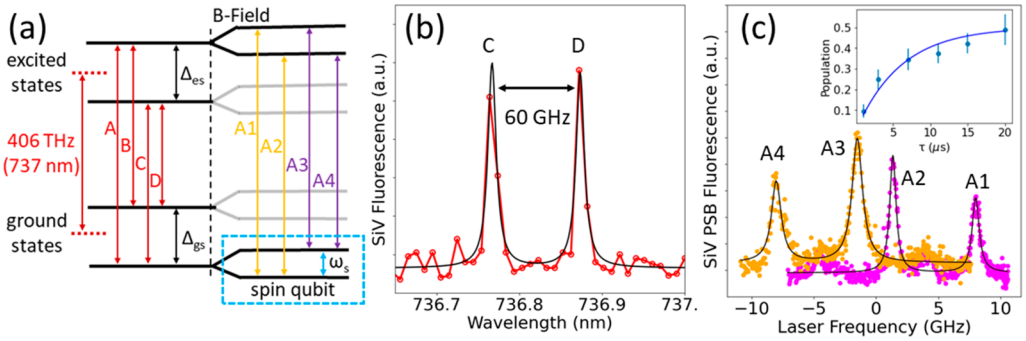

Figure 4. (a) Energy level diagram of the relevant SiV states. (b) Optical spectrum of the zero magnetic field SiV ZPL resonance fluorescence when pumping the A-line with 500 nW of power at the sample. (c) Photoluminescence excitation (PLE) spectrum of the SiV A-line spin-selective optical transitions in the presence of a 0.4 T z-axis magnetic field (misaligned from the SiV axis by 54.7°); the average optical line width is 815 MHz. Laser frequency is defined relative to the zero magnetic field A-line transition frequency. The inset shows the population recovery of the SiV spin qubit measured with a pump−probe technique on the A2 and A3 transitions; the decay time constant T_1 is 6.1 ± 0.7 μs. The blue curve is a fit result based on an exponential function.

to fabricate sideband-resolved resonators with large sideband asymmetries.

Next, we characterized the diamond OMCs at millikelvin temperatures inside a dilution refrigerator (Bluefors LD250). The diamond sample is mounted to a sample assembly that is thermally connected to the mixing plate at a base temperature of ∼50 mK. The optical and mechanical resonances of the OMC are measured via a tapered optical fiber routed into the refrigerator. Figure 3(b) shows the measured PSD at ∼50 mK of the same device and the mechanical mode shown in Figure 2(c). The selected spectrum was taken with the laser tuned to the blue optomechanical sideband ($\Delta = \kappa/2$) and at a power level corresponding to an intracavity photon number of $n_c \sim 100$. We observe mechanical line widths as low as 13 ± 1 kHz, corresponding to $Q_{mech} \sim 440{,}000$, which is a record high value for diamond OMCs. As expected, the Q-factor is dramatically improved at millikelvin temperatures compared to that at room temperature due to the lack of multiphonon damping mechanisms at such a low temperature. We also investigated the laser power dependence of this mechanical line width when the laser is red and blue detuned from the optical resonance by $\pm\kappa/2$ in Figure 3(c). As expected, the line width broadens when the laser is red detuned and narrows when the laser is blue detuned. The intrinsic mechanical line width γ_i, obtained by averaging the blue and red detuned line widths, rises slightly with increasing n_c indicating that optical power induced thermal broadening may be a small effect. The optomechanical damping rate is shown in the inset of Figure 3(c); a linear fit yields the optomechanical coupling rate $g_{OM}/2\pi \sim 30.3 \pm 1.6$ kHz at the single photon and phonon level.[30] The difference between the measured and simulated (127.4 kHz) values could be due to deviations, asymmetries, and disorder in the fabricated device geometry, with respect to the nominal design. Finally, we performed optical spectroscopy for single SiV centers embedded in the same OMC device shown in Figure 2 and Figure 3 using a home-built confocal microscope setup with an objective lens (Attocube LT-APO-VISIR, NA = 0.82) incorporated into the dilution refrigerator [Figure 3(a)]. Figure 4(a) shows the SiV energy level structure. There are two orbital levels in the ground state and two in the excited state, resulting in four optical transitions labeled A−D. Figure 4(b) shows the resonance fluorescence spectrum of an SiV center when a laser is resonantly excited at the A transition. We clearly observed emission in the corresponding C and D transitions originating from the same SiV center. From the distance between C and D transition lines, we infer a ground state splitting $\Delta_{gs} \sim 60$ GHz, which is slightly larger than the zero-strain value of ∼46 GHz.[9] This indicates that the SiV is slightly strained, likely due to residual strain induced by ion implantation or nanostructuring.[9,16] Low-strain SiV centers are advantageous for efficiently coupling to mechanical motion since the strain susceptibility of the spin transition decreases with increasing strain.[3,9] To perform spin spectroscopy on the same SiV center, we then applied a 0.4 T magnetic field along the lab z-axis (54.7° from the SiV axis), which further splits each energy level into two due to the spin 1/2 of the SiV. This in turn splits each optical transition in four. To carry out photoluminescence excitation (PLE) measurements of SiV centers, we scanned a tunable laser over the zero-phonon line (ZPL) transitions [named A−D in Figure 4(a)] using a tunable CW Ti:sapphire laser (M Squared). We also used a 520 nm green laser for periodically repumping the sample to maintain the charge state of the SiV.[16] Figure 4(c) displays the high-resolution PLE spectrum measured for the A transition, showing four peaks (named A1−A4) resulting from Zeeman splitting of the A transition under a magnetic field. In these measurements, we used a second tunable CW laser to repump one of the spin-dependent optical transitions and increase the visibility of other transitions. PLE resonances from A1 (A3) and A2 (A4) transitions are clearly observed by scanning the first CW laser, while the stationary repump laser is resonant with the A3 (A2) transition. To examine the spin properties of the SiV centers, we conduct spin lifetime (T_1) measurements on A3 using a pump−probe technique,[21] consisting of initialization and read-out pulses with a variable interpulse time delay, while a repump pulsed laser is tuned to the A2 transition (see details in the Supporting Information). The inset of Figure 4(c) shows the population recovery from the initialized spin state to the other spin state as a function of the interpulse delay time. The observed T_1 is 6.1 ± 0.7 μs, which is much shorter than the expected value of milliseconds at millikelvin temperatures for highly transverse magnetic fields.[3,33] A likely reason for the reduced spin T_1 is confocal-laser-induced heating of the local environment of the SiV center. Such heating can lead to elevated thermal occupation of the high frequency (∼50 GHz) phonon modes responsible for incoherent transitions between the ground state orbital levels, and thereby a reduction in spin T_1.[9] Note that telecom laser

https://doi.org/10.1021/acs.nanolett.3c04953
Nano Lett. 2024, 24, 6831−6837

power input via the tapered waveguide led to an unexpected SiV fluorescence quenching[8] (see the Supporting Information). To mitigate the effects of laser-induced heating on SiV centers, it is essential to reduce the necessary optical probe power required for SiV control and read-out. Indeed, cavity QED experiments with SiV centers[26] accomplish this by embedding SiV centers in photonic crystal cavities which support resonances close to SiV ZPL transitions (737 nm) and delivering probe signals via a tapered optical fiber interface. This reduces the laser probe powers to sub-nW levels,[26] which is orders of magnitude smaller than the power directed to SiV centers in our experiments (~1 μW). We note that this was not possible in our work where the optical cavity is designed to operate at telecommunication wavelengths, far detuned from the SiV center's ZPL. As a result, for the devices used in this work, optical excitation and collection of SiV fluorescence through the diamond waveguide port is less efficient than it is through the confocal microscope. Future work will focus on realizing diamond OMCs with optical resonances near the 737 nm wavelength range which will allow for efficient and resonantly enhanced excitation, control, and read-out of SiV centers via a tapered optical fiber interface, to minimize optical probe heating effects. Furthermore, 2D structures realized in recently demonstrated diamond membranes[34] could be utilized to increase the thermal conductivity between an OMC device and its cold thermal bath, thus minimizing heating effects.[35] With the reduced heating expected from these new designs, we expect to detect signatures of the acoustic resonance of the OMC in spin spectroscopy.

In summary, we have demonstrated high-Q diamond OMC devices with single SiV centers and measured a high-frequency (~6 GHz) mechanical mode with a line width of 13 ± 1 kHz ($Q \sim 4.4 \times 10^5$) at millikelvin temperatures, within an order of magnitude of state-of-the art line widths in silicon OMCs.[23] The usage of phononic bandgap shields between the OMC and the bulk substrate could further improve the mechanical Q-factors.[23] The pump power dependence of this line width allowed us to measure an optomechanical coupling rate of 30.3 ± 1.6 kHz at the single photon and phonon level, a value comparable with previous diamond OMCs. We confirmed that single SiV centers can maintain good optical properties even in the nanocavity and that their spins can be initialized and read out. From the pump power dependence of the OMC mechanical line width and spin lifetime measurements, we found that the coherence of the SiV spin and the OMC mechanical mode could be negatively impacted by laser-induced heating. The use of an efficient tapered diamond waveguide−tapered optical fiber interface[28] and of optical cavities resonant with the SiV ZPL[26] could greatly reduce optical probe powers and the associated heating. Based on the minimum measured mechanical line width $\kappa = 13 \pm 1$ (kHz), typical SiV spin decoherence rates ($\gamma \sim 100$ Hz),[21] and the simulated spin−phonon coupling rate $g_{SP}/2\pi$ (1.65 MHz), our OMC system could reach the strong spin−phonon coupling regime where $g_{SP} > \kappa, \gamma$. With reduced optical heating effects, we envision that high Q-factor diamond OMCs with SiV centers will allow the investigation of spin−phonon interactions in highly engineered acoustic structures and enable phonon-mediated interfaces between spins and other quantum platforms.

■ ASSOCIATED CONTENT

Supporting Information

The Supporting Information is available free of charge at https://pubs.acs.org/doi/10.1021/acs.nanolett.3c04953.

Optical and mechanical simulation details, device fabrication details, fluorescence quenching observation, pump−probe measurement details, integrated mechanical spectra vs intracavity photon number and mechanical quality factor discussion, and measurement setup details (PDF)

■ AUTHOR INFORMATION

Corresponding Author

Marko Lončar − *John A. Paulson School of Engineering and Applied Sciences, Harvard University, Cambridge, Massachusetts 02138, United States*; Email: loncar@seas.harvard.edu

Authors

Graham Joe − *John A. Paulson School of Engineering and Applied Sciences, Harvard University, Cambridge, Massachusetts 02138, United States*; orcid.org/0009-0003-3690-0561

Cleaven Chia − *John A. Paulson School of Engineering and Applied Sciences, Harvard University, Cambridge, Massachusetts 02138, United States; Institute of Materials Research and Engineering (IMRE), Agency for Science, Technology and Research (A*STAR), Singapore 138634, Republic of Singapore*

Benjamin Pingault − *John A. Paulson School of Engineering and Applied Sciences, Harvard University, Cambridge, Massachusetts 02138, United States; QuTech, Delft University of Technology, 2600 GA Delft, The Netherlands; Center for Molecular Engineering and Materials Science Division, Argonne National Laboratory, Lemont, Illinois 60439, United States*

Michael Haas − *John A. Paulson School of Engineering and Applied Sciences, Harvard University, Cambridge, Massachusetts 02138, United States*

Michelle Chalupnik − *John A. Paulson School of Engineering and Applied Sciences, Harvard University, Cambridge, Massachusetts 02138, United States*

Eliza Cornell − *John A. Paulson School of Engineering and Applied Sciences, Harvard University, Cambridge, Massachusetts 02138, United States*

Kazuhiro Kuruma − *John A. Paulson School of Engineering and Applied Sciences, Harvard University, Cambridge, Massachusetts 02138, United States*

Bartholomeus Machielse − *Department of Physics, Harvard University, Cambridge, Massachusetts 02138, United States*

Neil Sinclair − *John A. Paulson School of Engineering and Applied Sciences, Harvard University, Cambridge, Massachusetts 02138, United States*

Srujan Meesala − *Institute for Quantum Information and Matter and Thomas J. Watson, Sr., Laboratory of Applied Physics, California Institute of Technology, Pasadena, California 91125, United States*

Complete contact information is available at: https://pubs.acs.org/10.1021/acs.nanolett.3c04953

Author Contributions

[▽]G.J and C.C contributed equally to this paper.

https://doi.org/10.1021/acs.nanolett.3c04953
Nano Lett. 2024, 24, 6831−6837

Notes

The authors declare the following competing financial interest(s): B.M. is involved in developing diamond technologies at Amazon Web Services (AWS).

■ ACKNOWLEDGMENTS

The authors would like to thank M. Bhaskar, D. Assumpcao, and C. Knaut for the useful discussions. G.J. was supported in part by the Natural Sciences and Research Council of Canada (NSERC). C.C. was supported in part by Singapore's Agency for Science, Technology and Research (A*STAR). B.P. acknowledges financial support through a Horizon 2020 Marie Skłodowska-Curie Actions global fellowship (COHE-SiV, Project No. 840968) from the European Commission and through Q-NEXT, supported by the U.S. Department of Energy, Office of Science, National Quantum Information Science Research Centers. K.K. acknowledges financial support from JSPS Overseas Research Fellowships (Project No. 202160592). S.M. acknowledges support from the IQIM Postdoctoral Fellowship. Research funding: NSF Engineering Research Center for Quantum Networks (EEC-1941583), NSF Science and Technology Center for Integrated Quantum Materials (NSF DMR-1231319), AFOSR (FA9550-20-1-01015 and FA9550-23-1-0333), ARO (W911NF1810432), ONR (N00014-20-1-2425), and Harvard Quantum Initiative (HQI). This work was performed in part at the Center for Nanoscale Systems (CNS), a member of the National Nanotechnology Infrastructure Network (NNIN), which is supported by the National Science Foundation award ECS-0335765. CNS is part of Harvard University.

■ REFERENCES

(1) Manenti, R.; Kockum, A. F.; Patterson, A.; Behrle, T.; Rahamim, J.; Tancredi, G.; Nori, F.; Leek, P. J. Circuit quantum acousto-dynamics with surface acoustic waves,". *Nat. Commun.* **2017**, *8*, 975.

(2) Golter, D. A.; Oo, T.; Amezcua, M.; Lekavicius, I.; Stewart, K. A.; Wang, H. Coupling a Surface Acoustic Wave to an Electron Spin in Diamond via a Dark State,". *Phys. Rev. X* **2016**, *6*, 041060.

(3) Maity, S.; Shao, L.; Bogdanović, S.; Meesala, S.; Sohn, Y.-I.; Sinclair, N.; Pingault, B.; Chalupnik, M.; Chia, C.; Zheng, L.; Lai, K.; Lončar, M. Coherent acoustic control of a single silicon vacancy spin in diamond. *Nat. Commun.* **2020**, *11*, 193.

(4) Eichenfield, M.; Chan, J.; Camacho, R. M.; Vahala, K. J.; Painter, O. Optomechanical crystals. *Nature* **2009**, *462*, 78−82.

(5) Chan, J.; Alegre, T. P. M.; Safavi-Naeini, A. H.; Hill, J. T.; Krause, A.; Gröblacher, S.; Aspelmeyer, M.; Painter, O. Laser cooling of a nanomechanical oscillator into its quantum ground state. *Nature* **2011**, *478*, 89−92.

(6) Safavi-Naeini, A. H.; Gröblacher, S.; Hill, J. T.; Chan, J.; Aspelmeyer, M.; Painter, O. Squeezed light from a silicon micro-mechanical resonator. *Nature* **2013**, *500*, 185−189.

(7) Meesala, S.; Wood, S.; Lake, D.; Chiappina, P.; Zhong, C.; Beyer, A. D.; Shaw, M. D.; Jiang, L.; Painter, O. Non-classical microwave-optical photon pair generation with a chip-scale transducer. 2023, *arXiv preprint*, arXiv:2303.17684 [quant-ph], submitted on March 30, 2023. DOI: 10.48550/arXiv.2303.17684 (accessed February 21, 2024).

(8) Shandilya, P. K.; Lake, D. P.; Mitchell, M. J.; Sukachev, D. D.; Barclay, P. E. Optomechanical interface between telecom photons and spin quantum memory. *Nat. Phys.* **2021**, *17*, 1420−1425.

(9) Meesala, S.; Sohn, Y.-I.; Pingault, B.; Shao, L.; Atikian, H. A.; Holzgrafe, J.; Gündoğan, M.; Stavrakas, C.; Sipahigil, A.; Chia, C.; Evans, R.; Burek, M. J.; Zhang, M.; Wu, L.; Pacheco, J. L.; Abraham, J.; Bielejec, E.; Lukin, M. D.; Atatüre, M.; Lončar, M. Strain engineering of the silicon-vacancy center in diamond. *Phys. Rev. B* **2018**, *97*, 205444.

(10) Atatüre, M.; Englund, D.; Vamivakas, N.; Lee, S.-Y.; Wrachtrup, J. Material platforms for spin-based photonic quantum technologies. *Nat. Rev. Mater.* **2018**, *3*, 38−5.

(11) Zaitsev, A. M. *Optical Properties of Diamond: A Data Handbook*; Springer Science & Business Media: 2013.

(12) Tao, Y.; Boss, J. M.; Moores, B. A.; Degen, C. L. Single-crystal diamond nanomechanical resonators with quality factors exceeding one million. *Nat. Commun.* **2014**, *5*, 3638.

(13) Ovartchaiyapong, P.; Lee, K. W.; Myers, B. A.; Jayich, A. C. B. Dynamic strain-mediated coupling of a single diamond spin to a mechanical resonator. *Nat. Commun.* **2014**, *5*, 4429.

(14) Meesala, S.; Sohn, Y.-I.; Atikian, H. A.; Kim, S.; Burek, M. J.; Choy, J. T.; Lončar, M. Enhanced Strain Coupling of Nitrogen-Vacancy Spins to Nanoscale Diamond Cantilevers. *Phys. Rev. Appl.* **2016**, *5*, 034010.

(15) Chen, H.; Opondo, N. F.; Jiang, B.; MacQuarrie, E. R.; Daveau, R. S.; Bhave, S. A.; Fuchs, G. D. Engineering Electron-Phonon Coupling of Quantum Defects to a Semiconfocal Acoustic Resonator. *Nano Lett.* **2019**, *19*, 7021−7027.

(16) Sohn, Y.-I.; Meesala, S.; Pingault, B.; Atikian, H. A.; Holzgrafe, J.; Gündoğan, M.; Stavrakas, C.; Stanley, M. J.; Sipahigil, A.; Choi, J.; Zhang, M.; Pacheco, J. L.; Abraham, J.; Bielejec, E.; Lukin, M. D.; Atatüre, M.; Lončar, M. Controlling the coherence of a diamond spin qubit through its strain environment. *Nat. Commun.* **2018**, *9*, 2012.

(17) Maity, S.; Pingault, B.; Joe, G.; Chalupnik, M.; Assumpção, D.; Cornell, E.; Shao, L.; Lončar, M. Mechanical Control of a Single Nuclear Spin. *Phys. Rev. X* **2022**, *12*, 011056.

(18) Sipahigil, A.; Jahnke, K. D.; Rogers, L. J.; Teraji, T.; Isoya, J.; Zibrov, A. S.; Jelezko, F.; Lukin, M. D. Indistinguishable Photons from Separated Silicon-Vacancy Centers in Diamond. *Phys. Rev. Lett.* **2014**, *113*, 113602.

(19) Burek, M. J.; Cohen, J. D.; Meenehan, S. M.; El-Sawah, N.; Chia, C.; Ruelle, T.; Meesala, S.; Rochman, J.; Atikian, H. A.; Markham, M.; Twitchen, D. J.; Lukin, M. D.; Painter, O.; Lončar, M. Diamond optomechanical crystals. *Optica* **2016**, *3*, 1404−1411.

(20) Cady, J. V.; Michel, O.; Lee, K. W.; Patel, R. N.; Sarabalis, C. J.; Safavi-Naeini, A. H.; Jayich, A. C. B. Diamond optomechanical crystals with embedded nitrogen-vacancy centers. *Quantum Sci. Technol.* **2019**, *4*, 024009.

(21) Sukachev, D. D.; Sipahigil, A.; Nguyen, C. T.; Bhaskar, M. K.; Evans, R. E.; Jelezko, F.; Lukin, M. D. Silicon-Vacancy Spin Qubit in Diamond: A Quantum Memory Exceeding 10 ms with Single-Shot State Readout. *Phys. Rev. Lett.* **2017**, *119*, 223602.

(22) Atikian, H. A.; Latawiec, P.; Burek, M. J.; Sohn, Y.-I.; Meesala, S.; Gravel, N.; Kouki, A. B.; Lončar, M. Freestanding nanostructures via reactive ion beam angled etching. *APL Photonics* **2017**, *2*, 051301.

(23) MacCabe, G. S.; Ren, H.; Luo, J.; Cohen, J. D.; Zhou, H.; Sipahigil, A.; Mirhosseini, M.; Painter, O. Nano-acoustic resonator with ultralong phonon lifetime. *Science* **2020**, *370*, 840−843.

(24) Stockill, R.; Forsch, M.; Beaudoin, G.; Pantzas, K.; Sagnes, I.; Braive, R.; Gröblacher, S. Gallium Phosphide as a Piezoelectric Platform for Quantum Optomechanics. *Phys. Rev. Lett.* **2019**, *123*, 163602.

(25) Chia, C.; Machielse, B.; Shams-Ansari, A.; Lončar, M. Development of hard masks for reactive ion beam angled etching of diamond. *Opt. Express* **2022**, *30*, 14189−14201.

(26) Nguyen, C. T.; Sukachev, D. D.; Bhaskar, M. K.; Machielse, B.; Levonian, D. S.; Knall, E. N.; Stroganov, P.; Chia, C.; Burek, M. J.; Riedinger, R.; Park, H.; Lončar, M.; Lukin, M. D. An integrated nanophotonic quantum register based on silicon-vacancy spins in diamond. *Phys. Rev. B* **2019**, *100*, 165428.

(27) Evans, R. E.; Bhaskar, M. K.; Sukachev, D. D.; Nguyen, C. T.; Sipahigil, A.; Burek, M. J.; Machielse, B.; Zhang, G. H.; Zibrov, A. S.; Bielejec, E.; Park, H.; Lončar, M.; Lukin, M. D. Photon-mediated interactions between quantum emitters in a diamond nanocavity. *Science* **2018**, *362*, 662−665.

(28) Burek, M. J.; Meuwly, C.; Evans, R. E.; Bhaskar, M. K.; Sipahigil, A.; Meesala, S.; Machielse, B.; Sukachev, D. D.; Nguyen, C. T.; Pacheco, J. L.; Bielejec, E.; Lukin, M. D.; Lončar, M. Fiber-

https://doi.org/10.1021/acs.nanolett.3c04953
Nano Lett. 2024, 24, 6831−6837

Coupled Diamond Quantum Nanophotonic Interface. *Phys. Rev. Appl.* **2017**, *8*, 024026.
(29) Cohen, J. D.; Meenehan, S. M.; MacCabe, G. S.; Gröblacher, S.; Safavi-Naeini, A. H.; Marsili, F.; Shaw, M. D.; Painter, O. Phonon counting and intensity interferometry of a nanomechanical resonator. *Nature* **2015**, *520*, 522−525.
(30) Aspelmeyer, M.; Kippenberg, T. J.; Marquardt, F. Cavity optomechanics. *Rev. Mod. Phys.* **2014**, *86*, 1391−1452.
(31) Alegre, T. P. M.; Safavi-Naeini, A. H.; Winger, M.; Painter, O. Quasi-two-dimensional optomechanical crystals with a complete phononic bandgap. *Opt. Express* **2011**, *19*, 5658.
(32) Kippenberg, T. J.; Vahala, K. J. Cavity Optomechanics: Back-Action at the Mesoscale. *Science* **2008**, *321*, 1172−1176.
(33) Knall, E. N.; Knaut, C. M.; Bekenstein, R.; Assumpcao, D. R.; Stroganov, P. L.; Gong, W.; Huan, Y. Q.; Stas, P.-J.; Machielse, B.; Chalupnik, M.; Levonian, D.; Suleymanzade, A.; Riedinger, R.; Park, H.; Lončar, M.; Bhaskar, M. K.; Lukin, M. D. Efficient Source of Shaped Single Photons Based on an Integrated Diamond Nanophotonic System. *Phys. Rev. Lett.* **2022**, *129*, 053603.
(34) Guo, X.; Delegan, N.; Karsch, J. C.; Li, Z.; Liu, T.; Shreiner, R.; Butcher, A.; Awschalom, D. D.; Heremans, F. J.; High, A. A. Tunable and Transferable Diamond Membranes for Integrated Quantum Technologies. *Nano Lett.* **2021**, *21*, 10392−10399.
(35) Ren, H.; Matheny, M. H.; MacCabe, G. S.; Luo, J.; Pfeifer, H.; Mirhosseini, M.; Painter, O. Two-dimensional optomechanical crystal cavity with high quantum cooperativity. *Nat. Commun.* **2020**, *11*, 3373.

https://doi.org/10.1021/acs.nanolett.3c04953
Nano Lett. 2024, 24, 6831−6837